Three-dimensional stress effects on time-dependent swelling behaviour of shaly rocks

B.C. Hawlader, Y.N. Lee, and K.Y. Lo

Abstract: This paper presents a time-dependent constitutive model that has been developed for the swelling of shaly rocks. Laboratory test results on many shales, including Queenston shale, show that the swelling of these rocks depends on the applied stresses. The applied stress in one principal stress direction reduces swelling strain not only in that direction but also in the perpendicular directions. It was found that swelling strain reductions are nonlinearly dependent on applied stress. The reduction in lateral swelling caused as a result of axial stress is modeled using the "pseudo-Poisson's effect". The proposed model is used to simulate the development of swelling strain with time under uniaxial and biaxial stress conditions. Comparison between the computed and experimental results shows that the pseudo-Poisson's effect is a key parameter for simulating the observed time-dependent swelling.

Key words: swelling, Queenston shale, modeling, three-dimensional stress effect, nonlinearity.

Résumé : Cet article présente un modèle de comportement en fonction du temps qui a été développé pour le gonflement de roches schisteuses. Les résultats d'essais de laboratoire sur plusieurs schistes, incluant le schiste de Queenston, montrent que le gonflement de ces roches dépend des contraintes appliquées. La contrainte appliquée dans une direction de contrainte principale réduit la déformation en gonflement non seulement dans cette direction, mais aussi dans les directions perpendiculaires. On a trouvé que les réductions de la déformation en gonflement ont une dépendance non linéaire de la contrainte appliquée. La réduction du gonflement latéral causé par la contrainte axiale est modélisée au moyen du « pseudo-effet de Poisson ». Le modèle proposé est utilisé pour simuler le développement de la déformation du gonflement en fonction du temps sous des conditions de contraintes uniaxiales et bisaxiales. La comparaison entre les résultats calculés et expérimentaux montre que le pseudo-effet de Poisson est un paramètre clé pour simuler le gonflement observé qui dépend du temps.

Mots clés : gonflement, schiste de Queenston, modélisation, effet de contrainte tridimensionnelle, non linéarité.

[Traduit par la Rédaction]

Introduction

The occurrences of tunnel convergence, increase in lining stress, and in some cases, the destruction of linings caused by the swelling of rock are well known (Einstein 1989; Lo et al. 1978; Lo 1986; Lo and Yuen 1981). Lo and Yuen (1981) summarized the short- and long-term consequences of high in situ stress- and time-dependent deformation from a number of case records. In general, in situ stress-related problems in southern Ontario are caused by the high horizontal stress components (Lo 1978). The movement of bedding planes, heaving and buckling of the floor, and "local failure" at the crown and invert are common short-term problems in construction in soft rock. Short-term problems in tunneling and underground mining are usually overcome by providing adequate temporary support at appropriate times and locations and (or) by changing the geometry, shape, excavation sequence, and orientation of underground structures. On the other hand, long-term effects can include the convergence of an unsupported excavation or stress increase in a tunnel lining. In tunnels built in shales, this distress is manifested in the form of subhorizontal cracks at the springline (Lo and Yuen 1981). Einstein (1989) also reported a number of swelling cases, involving invert heave and crown displacements, of tunnels in Europe. An extreme case involved some critical sections of the Kappelesberg Tunnel where 15 ft (4.7 m) of total invert heave was observed.

Ontario Hydro planned the development of the Sir Adam Beck Niagara Generating Station (SABNGS) No. 3, later renamed the Niagara River Hydroelectric Development Project, near existing Generating Stations No. 1 and No. 2. This project consists of a tunnel 12 m in diameter and 10 km long, together with a powerhouse and auxiliary structures. The tunnel is to be located in Queenston shale. Lo and Lee (1990) showed that this shale has a very high swelling tendency that could damage the structures.

The swelling deformation of rock depends on the sustained stress components on it (Lo 1986). Field measurements and the performance of the structures in Queenston

Received 28 May 2002. Accepted 5 December 2002. Published on the NRC Research Press Web site at http://cgj.nrc.ca on 25 April 2003.

B.C. Hawlader. C-CORE, Morrissey Road, St. John's, NL A1B 3X5, Canada.
Y.N. Lee. Hyundai Institute of Construction Technology, Hyundai Engineering and Construction Co., #102-4 Mabuk-Ri, Yongin-Si, Kyunggi-Do 449-710, South Korea.
K.Y. Lo.[1] Geotechnical Research Centre, Faculty of Engineering, University of Western Ontario, London, ON N6A 5B9, Canada.

[1]Corresponding author (e-mail: k.y.lo@uwo.ca).

 doi: 10.1139/T03-006

shale have shown that this rock is under an anisotropic in situ stress state, with high horizontal stress components. The swelling strain is also anisotropic because of the rock formation and the anisotropic stress distribution in the surrounding rock after excavation. For the design and construction of a tunnel in this rock, it is therefore necessary to investigate three-dimensional time-dependent swelling behaviour under field stress conditions.

Several time-independent swelling models have been developed in the past for the design of tunnels based on the so-called swelling law (e.g., Grob 1972; Einstein et al. 1972; Wittke and Pierau 1979). The International Society of Rock Mechanics (ISMR 1994) examined the swelling models available in the literature and concluded that while the swelling deformation and pressure may be predicted using available models, time-dependent swelling models needed to be developed from a fundamental knowledge of the swelling mechanism. Lo and Yuen (1981) and more recently Lo and Hefny (1996) developed rheological models for the time-dependent swelling behaviour of rock. These models were used in the design of underground structures in southern Ontario (e.g., Lo et al. 1986; Trow and Lo 1989). Although the performance records of as-built structures show that the solutions are adequate, these approaches are based on the generalization of uniaxial stress–strain–time relationships to the three-dimensional state utilizing the classical theory of viscoelasticity and therefore do not completely take into account the material behaviour under combined stress conditions. Also, these models cannot predict the very long time swelling deformation (up to 100 years) that is observed in the field (e.g., swelling of a wheelpit at Niagara Falls (Lee and Lo 1976)). Moreover, it is recognized that the predictions of these models may be overly conservative in some cases.

This paper consists of two parts. The first part describes the laboratory test results of the swelling deformation of Queenston shale in three orthogonal directions under different stress conditions. In the second part, a constitutive model is developed including the nonlinear three-dimensional stress dependency of long-term swelling. The theoretical results are then compared with the experimental data.

Laboratory test program

To characterize swelling behaviour, Lo and his coworkers (e.g., Lo et al. 1978, 1984; Lo 1986; Lee 1988; Huang 1993) performed comprehensive experimental studies on shaly rocks from southern Ontario. The test apparatus and the methods of measurement were originally developed by Lo et al. (1978). These simple but practical and effective testing techniques are capable of examining most of the swelling features that exist in these shales and are used extensively for design purposes. However, as mentioned before, the stresses in the rock before and after excavation are anisotropic in the field and the deformation behaviour is intrinsically anisotropic. It is therefore expected that the swelling strains are also anisotropic. Three-dimensional swelling behaviour is studied in this paper using the modified test apparatus developed by Lo and Lee (1990). Queenston shale rock samples obtained from the Niagara Falls area at depths between 80 and 122 m are used in this test program.

General properties of Queenston shale

Queenston shale is a reddish brown mudstone exhibiting cross-anisotropic elastic deformation behaviour. The Poisson's ratio on horizontal strain for vertical stress (≈ 0.35) is less than that of vertical strain for horizontal stresses (≈ 0.4). The Poisson's ratio for horizontal stress on horizontal strain is 0.26. The uniaxial compressive strengths of the vertical and the horizontal specimens are approximately the same. The vertical and horizontal elastic moduli are approximately 9 and 13 GPa, respectively. The average unit weight is 26.7 kN/m^3, and the specific gravity is 2.82 with a porosity of 7%. The calcite content varies from 3 to 7% (Lo and Lee 1990).

The swelling test and its mechanism

An extensive test program was carried out (Lee and Lo 1993) to investigate the sources and mechanism of the swelling behaviour of Queenston shale and other shales in southern Ontario. It was found that swelling of these shales occurs through the migration of moisture without any chemical changes, such as oxidation of sulfides to sulfates, hydration of anhydrite to gypsum, or the creation of new crystal structures (Wittke and Pierau 1979; Madsen and Nüesch 1991). These shales swell as a result of the dilution of pore water salt concentration, which increases the spacing between the clay particles. Both osmosis and diffusion are responsible for this dilution process. Water moves into the shale via negative pore pressure and the process of osmosis. It has also been found that the formation of cracks enhances the degree of swelling by facilitating water movement towards the central region of the sample. The above mentioned mechanisms are effective only when there is some stress relief. Underground excavation changes the initial state of stress providing the initiating mechanism for swelling deformation.

For the design and analysis of the proposed tunnel, Lee (1988) performed a series of swelling tests on Queenston shale. The test program included (*i*) free swell tests, (*ii*) modified semiconfined swelling tests under uniaxial stress, and (*iii*) biaxial swelling tests. All of the tests were conducted in a temperature controlled room (10±2°C).

The free swell test is the simplest form of swelling test. In this test, freshly trimmed cylindrical specimens are kept in ambient fluid and the deformations in three orthogonal directions are measured. This test gives the maximum possible swelling of the rock provided the other conditions are the same. As will be shown later, the free swelling strain has a good correlation with the swelling strain under different stress conditions.

The general arrangement of the modified semiconfined swelling test cell is similar to the semiconfined swelling test cell developed by Lo et al. (1978) but with additional lateral deformations in two orthogonal directions measured by strain gauges mounted on cantilever beams. Axial deformation is monitored using a dial gauge with 0.002 mm precision. The detailed arrangement of this system is shown in Fig. 1*a*.

In the biaxial swell test, a uniform pressure on the cylindrical surface is applied using a Hoek cell (Hoek and Brown

Fig. 1. (*a*) Modified semiconfined swelling test. (*b*) Swelling test under biaxial stress.

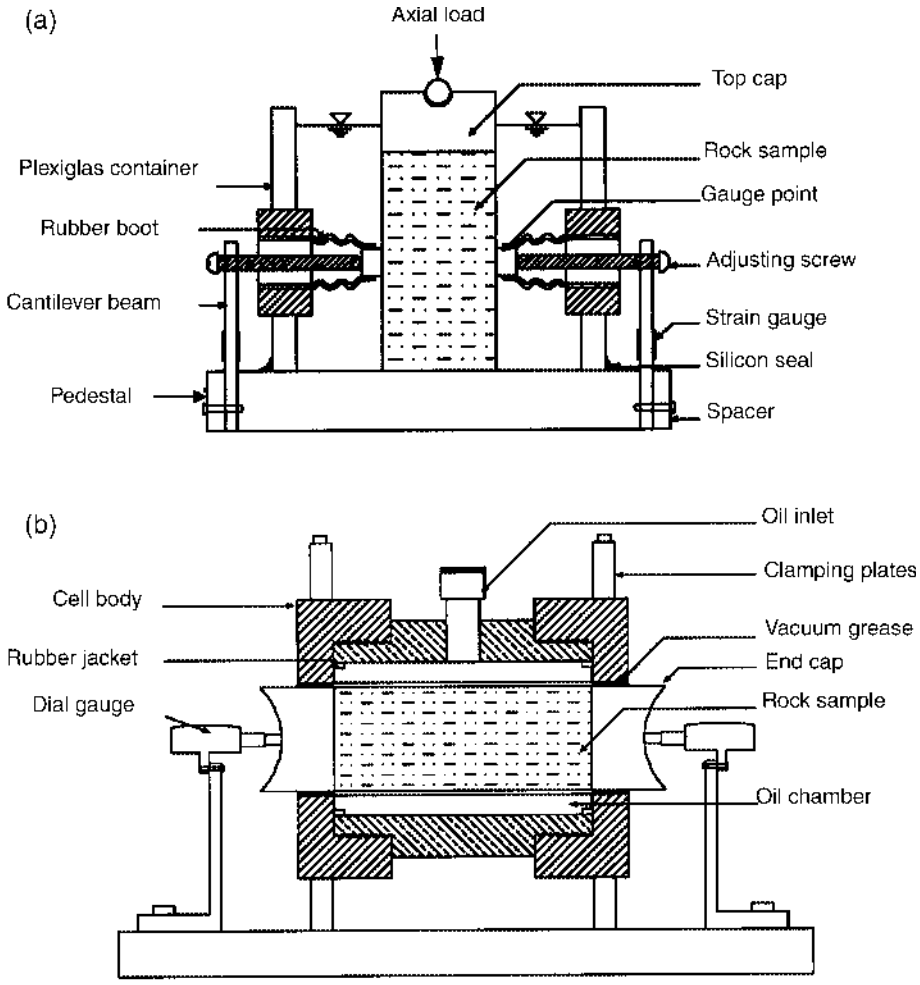

1980, Fig. 1*b*). The pressure is supplied by a hydraulic pump with a capacity of 30 MPa. The longitudinal deformations are measured using dial gauges and strain gauges, while the radial deformations are measured by strain gauges mounted on the specimen.

Tests were done on samples of different orientation to study the directional swelling behaviour. The symbol "*y*" (see Fig. 2) is used in this study to represent the axis perpendicular to the bedding plane. It also represents the vertical direction because the bedding planes are essentially horizontal. The symbol "*x*" represents the direction of the horizontal major principal stress while the symbol "*z*" is used for the direction of the horizontal minor principal stress. In modified semiconfined swelling tests and biaxial swelling tests, preselected constant stresses are applied in the *x*, *y*, *z* directions (Fig. 2).

Development of swelling strain

Typical swelling test results are shown in Fig. 3. In this figure, the development of swelling strain with time in three principal stress directions is plotted under different levels of stresses (σ_y = 0 i.e., free swell, to σ_y = 0.69 MPa) applied in the *y* direction. It can be seen from Fig. 3*a* that, neglecting the few points in the early stages of testing, the swelling behaviour in the direction of the applied stress can be represented by a straight line in a plot of swelling strain (ε_y) versus the logarithm of time (*t*). It takes some time from the start of the tests for the specimen to reach equilibrium once the specimen is moved from the environmental conditions in the field to those in the laboratory, and the results for the first few days are not used. The slope of this straight line is termed the "swelling potential" (Lo et al. 1978). This linear relationship holds not only for the free swell test but also for swelling under different σ_y, although the swelling potential reduces with σ_y. Figures 3*b* and 3*c* show that the ε–log*t* plots are also reasonably linear in the horizontal directions (*x* and *z*) under different magnitudes of stress applied in the vertical (*y*) direction. Similar behaviour was obtained from other series of tests, where the loads were applied in the *x* or *z* directions (Lee 1988).

Based on the above observation, the swelling strain at time *t* can be expressed as

$$[1] \qquad \varepsilon_i(t) = m_{i(s)} \log\left(\frac{t}{t_0}\right)$$

where *m* is the slope of the straight line. The subscript *i* represents the direction of the swelling, and *s* is used to define the stress levels. Swelling begins at the reference time t_0.

Fig. 2. Test program: (*a*) free swell; (*b*) modified semiconfined vertical (*y*); (*c*) modified semiconfined horizontal (*x*); (*d*) modified semiconfined horizontal (*z*); (*e*) biaxial stress.

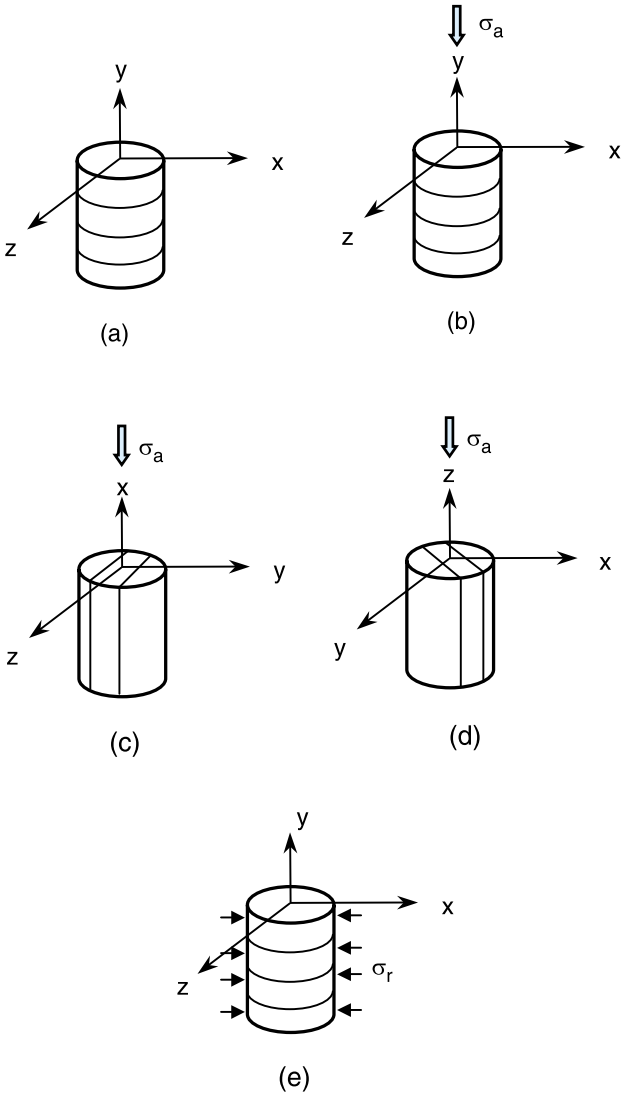

Effect of applied stress

Stress dependency of the swelling strain of Queenston shale has been confirmed by several researchers (e.g., Lo et al. 1978; Lo and Lee 1990). Horizontal and vertical swelling potentials for 11 free swell tests and 27 modified semiconfined swell tests are plotted in Fig. 4. It can be seen that the swelling potential is systematically higher in the vertical direction than in the horizontal direction. The swelling potential decreases linearly with the logarithm of applied stress. These figures show that the applied stress reduces the swelling potential not only in the loaded direction but also in its two orthogonal directions. For instance, a relatively small amount of vertical stress (≈0.02 MPa) reduces 30% of the free swell potential in the horizontal direction (Fig. 4*b*) with no external stresses applied. Similar behaviour is found for swelling in other directions (Figs. 4*a* and 4*c*). This behaviour is quite analogous to the Poisson's effect in elastic behaviour.

The swelling potentials in the loading directions only are plotted in Fig. 5. It can be seen that the swelling potential reduces to zero at a critical pressure (σ_c). A pressure equal to or greater than this suppresses all swelling mechanisms and no swelling deformation occurs. Moreover, σ_c is approximately the same for both the vertical and horizontal directions. The free swell test result is represented by a small stress (= 0.001 MPa) (Lee 1988) because swelling potentials are plotted against the logarithm of the applied stress. This stress is defined as the threshold stress (σ_{th}), which can be determined experimentally from semiconfined swell tests under very small pressures. For an applied stress less than σ_{th}, swelling strain at any time is the same as the free swelling strain. The suppression effect is effective only after σ_{th} is exceeded.

The swelling potentials under applied stresses are normalized with their corresponding values of free swell potentials and are plotted in Fig. 6. Both lines in Fig. 5 merge into one line (solid line in Fig. 6) because of this normalization. Normalized swelling potential in the direction of the applied stress can be represented by one line. The normalized swelling potential value is one at the free swelling condition and is zero at the critical pressure (σ_c). The percentage of reduction of swelling potential from its value at the free swell condition is also shown in Fig. 6. The reduction is zero at the free swell condition and is 100% at critical pressure σ_c. In the following sections the reduction of swelling potential will be used to model the stress effect on swelling.

Normalized swelling potential in the direction perpendicular to the applied stress is also shown in Fig. 6. The reduction in swelling potential is less in this direction. The reductions in the perpendicular direction differ and are dependent upon the swelling properties of the rock. However, only one line is drawn on this figure for clarity of discussion. The same relationship is applicable if swelling strain at any time (*t*) is used instead of swelling potential (see eq. [1]).

Proposed swelling model

The experimental results show that the applied stress in one direction restricts the swelling in the other two orthogonal directions. To illustrate this behaviour, consider a rock element in two dimensions as shown in Fig. 7*a*. The effect of three-dimensional stress will be discussed later. If this rock element swells without any application of external load (free swelling condition), it will swell in every direction as shown by the solid lines in Fig. 7*a*. The experiments show that the amount of swelling at a given time is different in each direction. In this case, free swelling strain in two perpendicular (*x* and *y*) directions is represented by $\varepsilon_{x(0)}$ and $\varepsilon_{y(0)}$, respectively. Note that the subscript "0" is used to represent the free swelling condition.

If the same sample is allowed to swell under an external stress σ_y in the *y* direction, the swelling behaviour will change. Swelling strain in the direction of the applied stress (*y*) is reduced by $\Delta\varepsilon_{y(\sigma_y)}$. Therefore, the swelling strain in the *y* direction under this stress is

$$[2] \qquad \varepsilon_y = \varepsilon_{y(0)} - \Delta\varepsilon_{y(\sigma_y)}$$

Fig. 3. Typical swelling strain time curve under different magnitudes of axial stress.

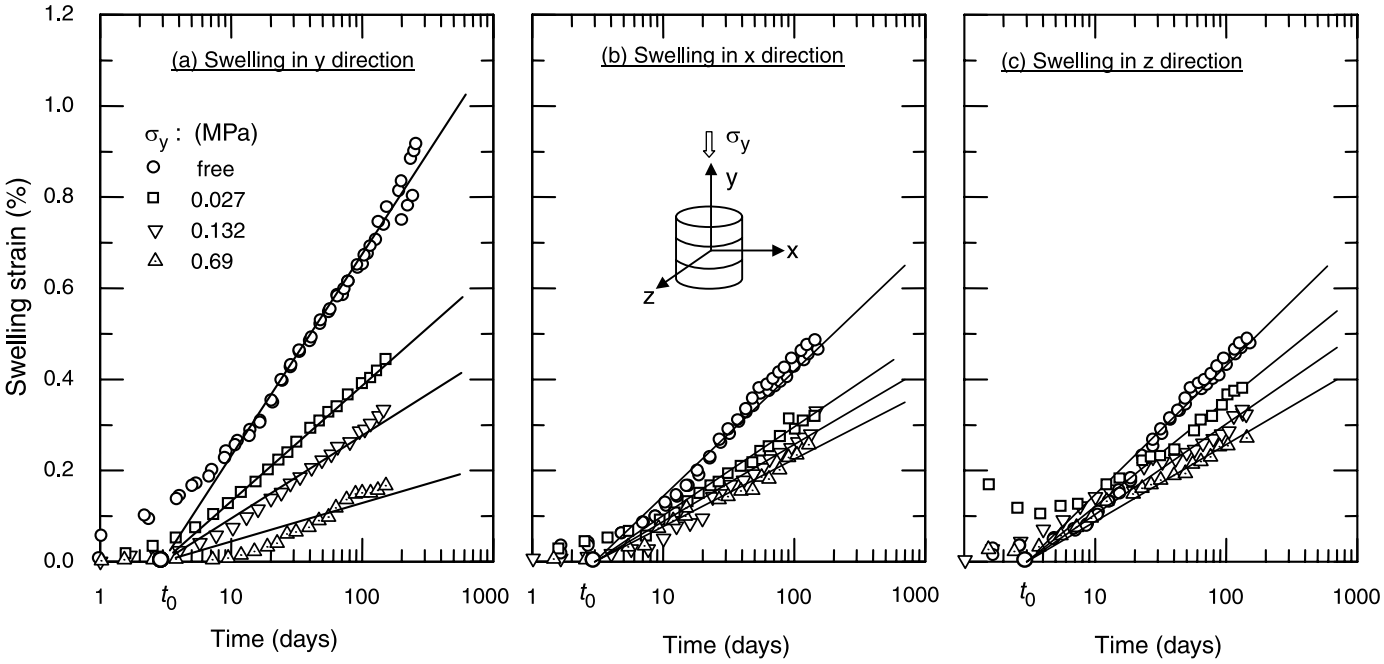

The swelling strain in the *x* direction (i.e., perpendicular to the direction of the applied stress) is also influenced by σ_y. As shown in Fig. 7*a*, swelling strain in the *x* direction is also reduced by $\Delta\varepsilon_{x(\sigma_y)}$ from the free swelling strain. The experimental results reveal that the percentage of swelling strain reduction under an applied stress (reduction of swelling strain/free swelling strain) is less in the orthogonal directions than in the direction of the applied stress (Fig. 6). For brevity, the term "reduction ratio" is used for the ratio of swelling strain reduction and free swelling strain in the following sections.

The reduction ratio is plotted against $\log\sigma_y$ in Fig. 7*b*, which is a linear function (see Fig. 6). The reduction of swelling strain is zero at the threshold stress (σ_{th}) and 100% at the critical stress (σ_c).

When the rock sample swells under σ_y, the reduction ratio in the *y* direction (R_{yy}) is (Fig. 6)

$$[3] \qquad R_{yy} = \frac{\Delta\varepsilon_{y(\sigma_y)}}{\varepsilon_{y(0)}} = \frac{\log\left(\frac{\sigma_y}{\sigma_{th}}\right)}{\log\left(\frac{\sigma_c}{\sigma_{th}}\right)}$$

The reduction ratio in the *x* direction is represented by

$$[4] \qquad R_{xy} = \frac{\Delta\varepsilon_{x(\sigma_y)}}{\varepsilon_{x(0)}} = \mu_{xy}R_{yy} = \mu_{xy}\frac{\Delta\varepsilon_{y(\sigma_y)}}{\varepsilon_{y(0)}}$$

where μ_{xy} is the "pseudo-Poisson's ratio". The subscripts (*x* and *y*) denote the effect on swelling strain reduction in the *x* direction for a load applied in the *y* direction.

It is useful to examine the concept of "virtual stress" as it is used in this study. The term virtual stress represents the amount of stress to be applied to reduce the swelling strain in the direction perpendicular to the direction of the applied stress. As an example, consider the rock element mentioned above (Fig. 7*a*). Swelling in the *x* direction is reduced by $\Delta\varepsilon_{x(\sigma_y)}$ for an applied stress σ_y in the *y* direction. Virtual stress σ^*_{xy} is a uniaxial stress that must be applied in the *x* direction to suppress the same amount of swelling ($\Delta\varepsilon_{x(\sigma_y)}$) in the *x* direction.

Once the reduction ratio in the *x* direction is known (eq. [4]), the virtual stress can be calculated as

$$[5] \qquad \sigma^*_{xy} = \sigma_{th}10^{[R_{xy}\log(\sigma_c/\sigma_{th})]}$$

where the first subscript (*x*) in virtual stress (σ^*_{xy}) is used to define the direction of virtual stress for an applied stress in the direction of the second subscript (*y*).

Extension of pseudo-Poisson's effect for the three-dimensional stress condition

The model discussed above can be used to predict the time-dependent swelling deformation under uniaxial stress. Since the problem of underground excavation involves three-dimensional stress changes, it is necessary to formulate the three-dimensional swelling behaviour of rock for field stress conditions. Consider a rock element that swells under three principal stresses (σ_x,σ_y,σ_z) as shown in Fig. 8. The effect of these stresses on swelling is superimposed as follows. First, the effect of σ_y on swelling strain is examined. Similar to the uniaxial loading effect discussed in the previous section, strain reduction can be calculated in three directions. Strain reductions perpendicular to the direction of the applied stress are calculated using the pseudo-Poisson's ratios obtained from uniaxial loading tests. In addition to R_{yy} and R_{xy} obtained from eqs. [3] and [4], respectively, the swelling strain reduction in the *z* direction (R_{zy}) is calculated as

Fig. 4. The effect of applied stress on swelling potential.

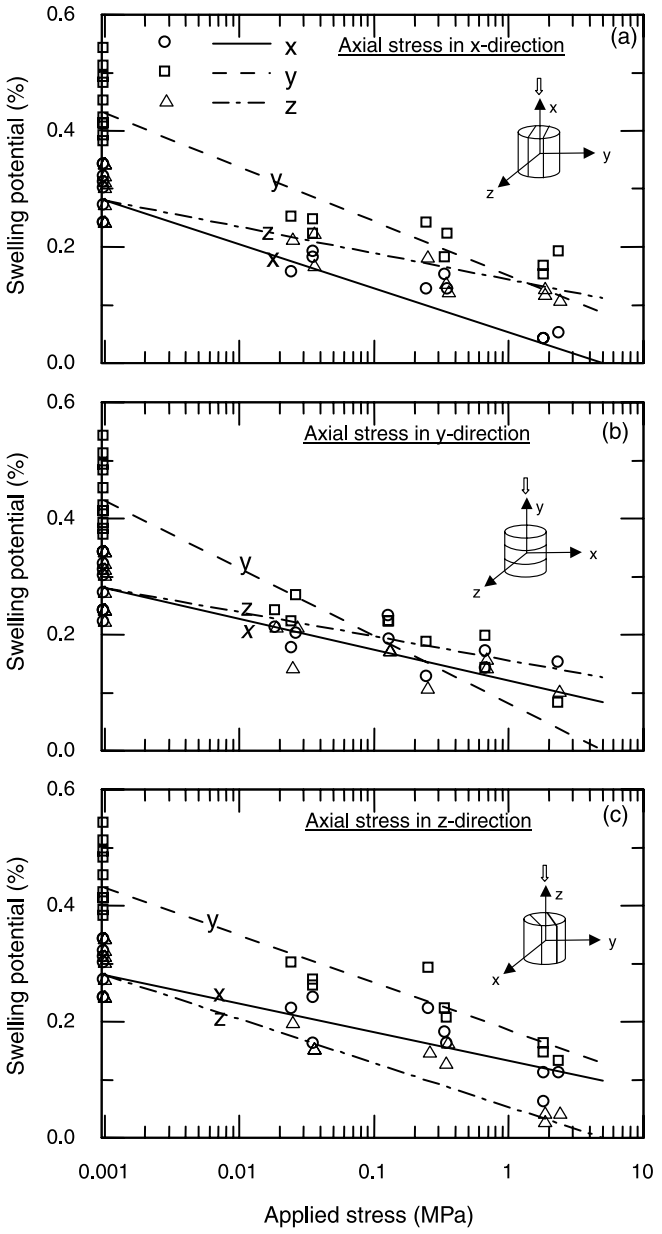

$$[6] \qquad R_{zy} = \frac{\Delta\varepsilon_{z(\sigma_y)}}{\varepsilon_{z(0)}} = \mu_{zy} R_{yy} = \mu_{zy} \frac{\Delta\varepsilon_{y(\sigma_y)}}{\varepsilon_{y(0)}}$$

Once the strain reductions in the x and z directions are known, the virtual stresses in two orthogonal directions of y (σ^*_{xy} and σ^*_{zy} in Fig. 8) corresponding to these strain reductions (R_{xy}, R_{zy}) are obtained as (see eq. [5])

$$[7] \qquad \sigma^*_{ij} = \sigma_{th} 10^{[R_{ij} \log(\sigma_c/\sigma_{th})]} \qquad (i = x, z \text{ and } j = y)$$

Similarly, the virtual stresses in the orthogonal directions for σ_x and σ_z can be calculated. Once the virtual stresses are known, the suppression stresses in three different directions are calculated as

$$[8] \qquad \sigma_i^{TS} = \sigma_i + (1 - \delta_{ij})\ \sigma^*_{ij}$$

Fig. 5. Stress effect in the direction of the applied stress.

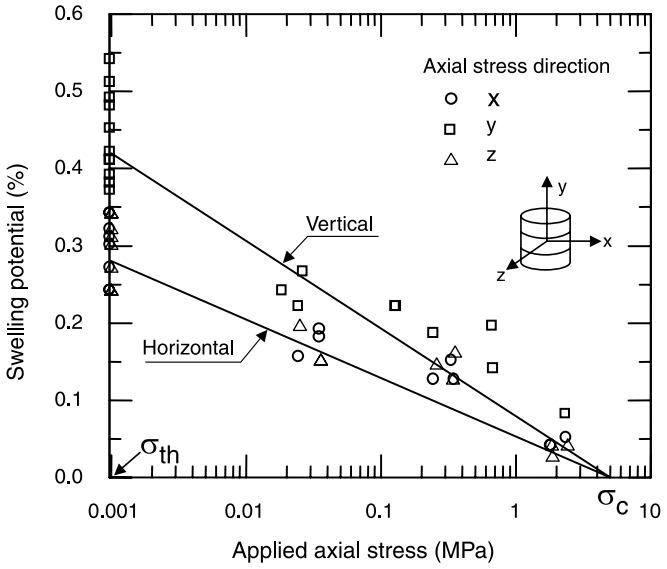

Fig. 6. Normalized swelling potential and its reduction.

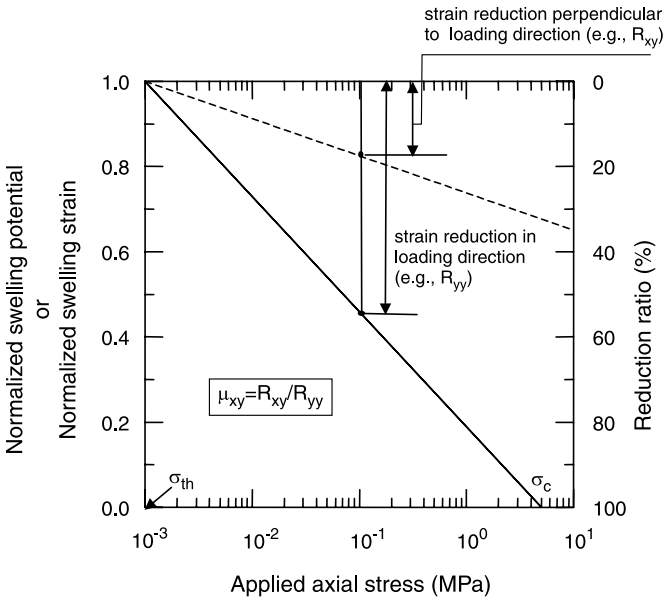

where the superscript "TS" is used to represent the resultant suppression stress for the three-dimensional stress condition; σ_i is the applied stress; subscripts i and j represent the x, y, and z directions; and δ_{ij} is the Kronecker delta and its components are 1 if $i = j$ and 0 if $i \neq j$.

Using σ_i^{TS} from eq. [8], the reduction of the swelling strain in the generalized stress state is obtained as

$$[9] \qquad R_i^{TS} = \frac{\log\left(\dfrac{\sigma_i^{TS}}{\sigma_{th}}\right)}{\log\left(\dfrac{\sigma_c}{\sigma_{th}}\right)}$$

Fig. 7. Swelling strain reduction under uniaxial stress. (*a*) Swelling in two dimensions under applied stress σ_y. (*b*) Modeling of swelling behaviour.

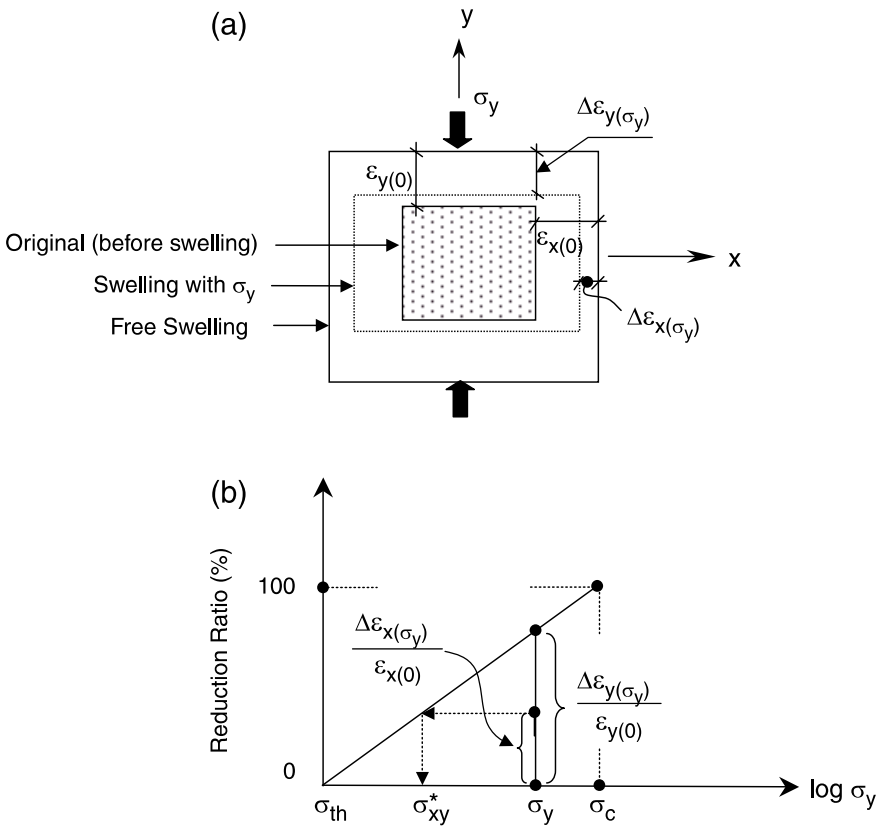

Fig. 8. Swelling strain reductions in three dimensions under the applied stress σ_y.

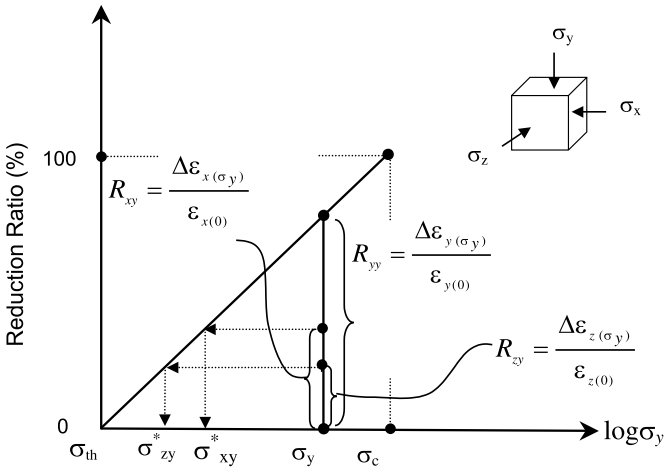

Finally, the swelling potential under a multiaxial stress system can be expressed as

$$[10] \quad m_{i(\sigma_{ij})} = (1 - R_i^{TS})\, m_{i(0)}$$

where $m_{i(\sigma_{ij})}$ is the swelling potential in the i direction under a three-dimensional stress state (σ_{ij}) and $m_{i(0)}$ is the free swelling potential.

Verification of proposed model

To verify the proposed model described in the previous section, different types of tests (Lee 1988) involving the development of swelling strain with time are used. An example of the procedure for calculating the time-dependent deformation of the specimens under different applied stress conditions is described in Appendix A.

First, a series of tests is considered where axial stress is applied in the vertical direction (Fig. 2*b*). The development of swelling strains in the *x*,*y*,*z* directions with time under different magnitudes of axial stresses in the *y* direction (σ_y = 0.0 (free), 0.27, 0.132, 0.69 MPa) are plotted in Fig. 9. It can be seen from Fig. 9 that the application of stress in the *y* direction reduces the swelling strain in all three directions. To simulate this behaviour, the free swelling potential in three different directions ($m_{x(0)}$, $m_{y(0)}$, $m_{z(0)}$) is obtained first from the free swell test results. The critical stress (σ_c) is obtained from the plot of the swelling potential versus the logarithm of the applied stress (Fig. 5). The pseudo-Poisson's ratios are then obtained from a plot such as the one shown in Fig. 6. The swelling strain is calculated using the above-mentioned procedure. The various input parameters used in the calculation are listed in Table 1. It can be seen that the predicted swelling strains match very well with the laboratory test results not only in the vertical direction where axial stress is applied but also in the horizontal directions, indicating the pseudo-Poisson's effect is satisfactorily simulated.

Fig. 9. Predicted and measured swelling strain for vertical (*y*) specimens (points, measured; solid lines, predicted).

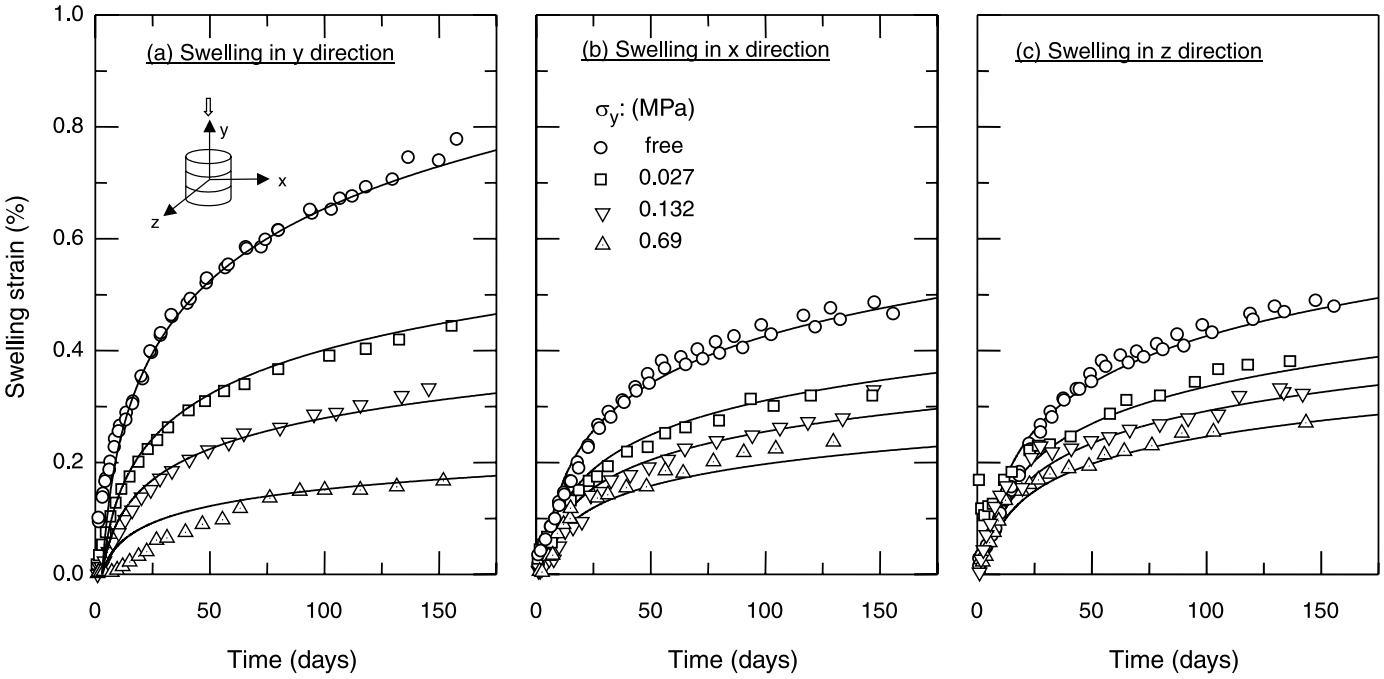

Fig. 10. Predicted and measured swelling strain for horizontal (*x*) specimens (points, measured; solid lines, predicted).

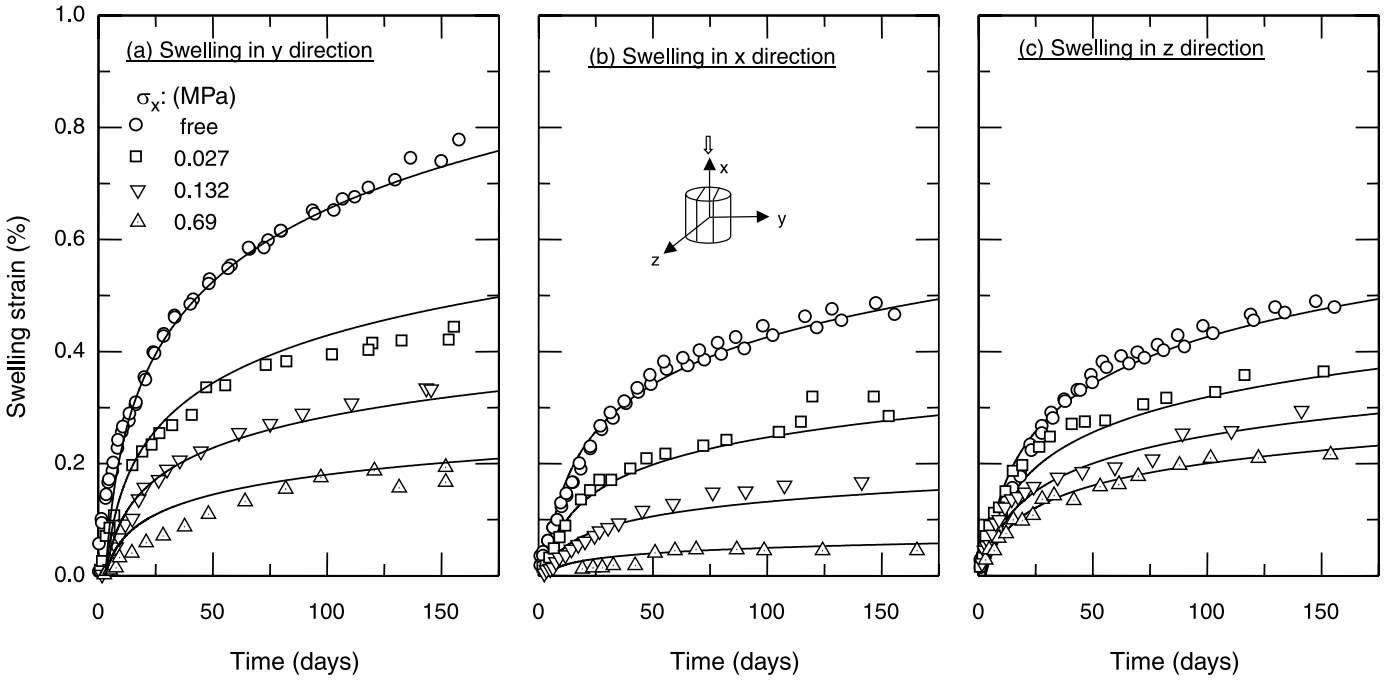

Figures 10 and 11 show the swelling strain development under axial stresses in the *x* and *z* direction (horizontal), respectively, (Figs. 2*c* and 2*d*). The predicted strain time curves for different applied stresses are also plotted in the same figures. It can be seen that the simulated curves are very close to the test results, which again confirms that the model is capable of simulating swelling strains in all three principal stress directions under uniaxial loading.

Simulation of the effect of biaxial stress on swelling is shown in Fig. 12. In this test, a uniform radial pressure of 4.5 MPa is applied on the cylindrical surface and no stress is applied in the longitudinal direction. The direction of loading is parallel to the bedding plane. It was found that, similar to the modified semiconfined swell tests where axial stresses reduce radial strain, the radial pressure reduces the swelling strain in the axial direction. In the simulation, the virtual stresses in the *y* direction (σ^*_{yx} and σ^*_{yz}) caused by the applied radial stress are calculated using eq. [7]. The resul-

Fig. 11. Predicted and measured swelling strain for horizontal (*z*) specimens (points, measured; solid lines, predicted).

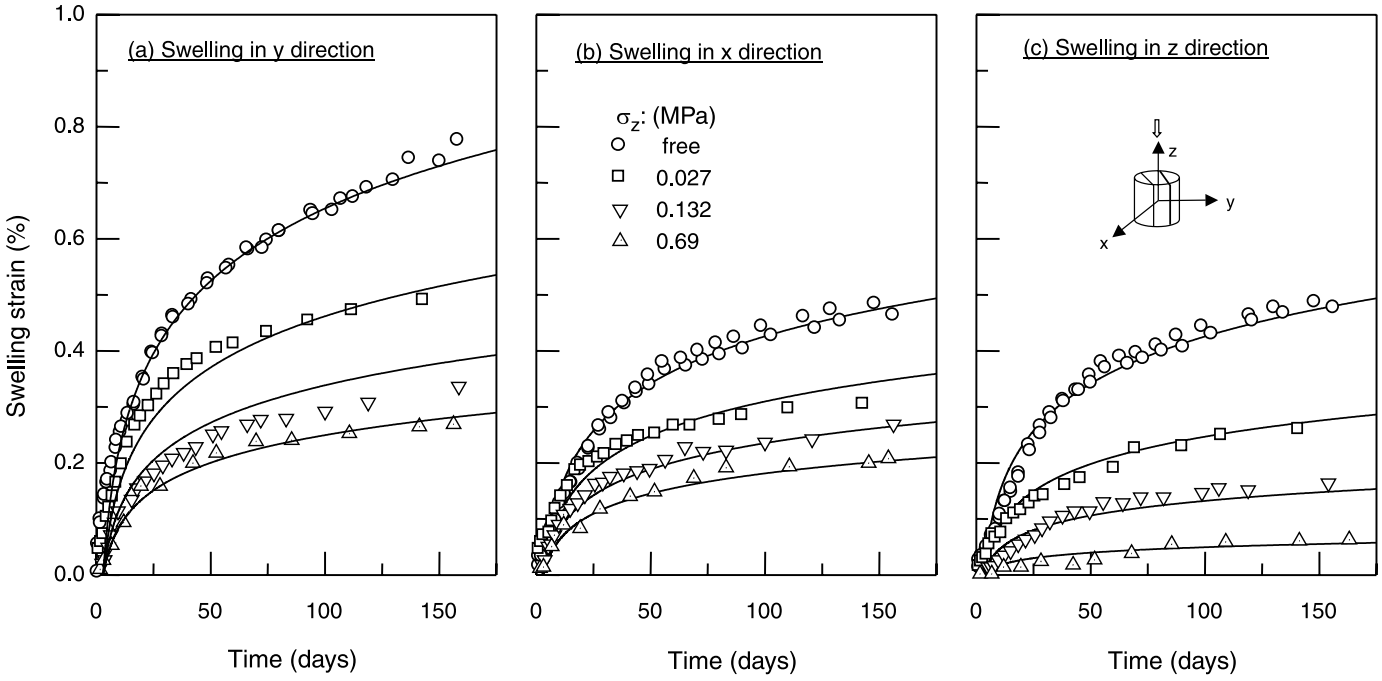

Table 1. Parameters used in computation.

Critical stress, σ_c (MPa)	5.0
Threshold stress, σ_{th} (MPa)	0.001
Reference time, t_0 (days)	3.0
Free swelling potentials	
$m_{x(0)}$	0.28
$m_{y(0)}$	0.43
$m_{z(0)}$	0.28
Pseudo-Poisson's ratios	
μ_{xy}	0.7
μ_{xz}	0.65
μ_{yx}	0.8
μ_{yz}	0.7
μ_{zx}	0.6
μ_{zy}	0.55

Fig. 12. Predicted and measured swelling strain for biaxial loading (points, measured; solid lines, predicted).

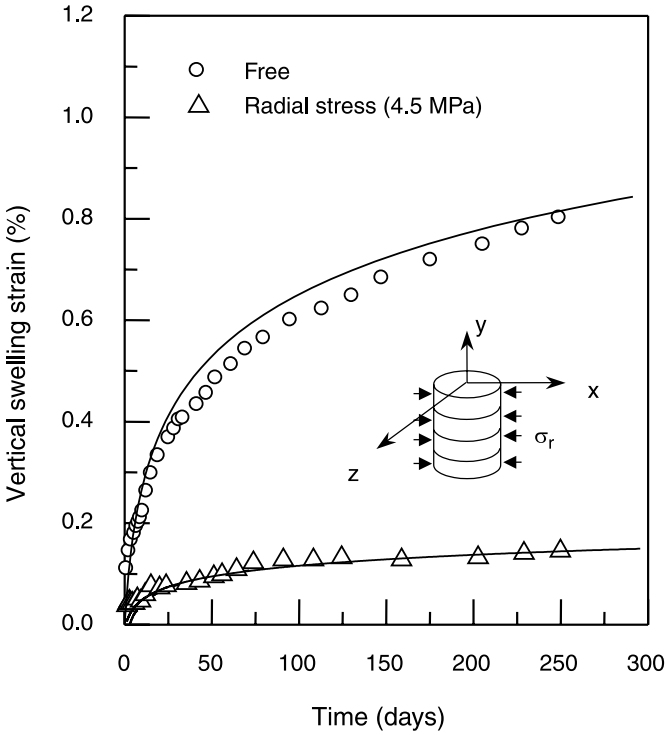

tant suppression effect is calculated using eq. [9]. It can also be seen from Fig. 12 that this model reasonably predicts the test results under the biaxial stress condition.

Application of proposed model

Time-dependent swelling deformation is an important issue in designing underground structures in shaly rocks in southern Ontario. Once excavation takes place, stress develops in the surrounding rock, which varies with radial distance from the tunnel. Stress also depends on the tangential position of the rock element because of anisotropic in situ stress distribution (Lo 1978; Franklin and Hungr 1977). Moreover, the time-dependent swelling deformation causes three-dimensional stress change in the rock as the stresses on the lining develop as a result of rock–structure interaction over time. The proposed model allows us to consider the effect of stress components in all three directions (see Fig. 6). The parameters needed in this model can be obtained from simple swelling tests (free swell tests and modified semi-confined swelling tests). This model has been successfully implemented in a finite element code to simulate the swell-

ing behaviour of rock at the Heart Lake storm sewer tunnel near the Pearson International Airport and the Darlington coldwater intake tunnel located at 60 km east of Toronto on the shore of Lake Ontario. It was found that the model simulates results of field observations more accurately. The numerical results will be published in another paper.

Conclusions

The main objective of the research presented in this paper is the development of a constitutive model for long-term swelling deformation of the shales in southern Ontario, taking into account three-dimensional stress effects. Extending the findings of Lo and Lee (1990) that the application of stress in one direction not only suppresses the swelling in that direction but also reduces the swelling in the orthogonal directions, it is shown that this "pseudo-Poisson's effect" can be modeled by the introduction of virtual stresses. The time-dependent deformations are then governed by 11 material parameters: the three free swell potentials ($m_{x(0)}$, $m_{y(0)}$, $m_{z(0)}$); the six pseudo-Poisson's ratios (μ_{xy}, μ_{xz}, μ_{yx}, μ_{yz}, μ_{zx}, μ_{zy}); the threshold stress (σ_{th}) below which no swelling strain reduction occurs; and the critical stress (σ_c) above which swelling is entirely suppressed. All of the parameters may be readily obtained from free swell and modified semiconfined swell tests.

The model was used to predict the swelling of rock in three principal stress directions under various applied stress conditions. The predicted results were compared with the measured swelling deformations under uniaxial and biaxial stresses. There was consistent agreement, clearly indicating that the proposed model is capable of predicting the swelling behaviour of shales under multiaxial stresses.

Acknowledgements

The study presented in this paper was supported by Ontario Hydro and the Natural Sciences and Engineering Research Council of Canada Grant No. R1121A01. The support is greatly appreciated.

References

Einstein, H.H. 1989. Design and analysis of underground structures in swelling and squeezing rocks. *In* Underground structures: design and instrumentation. *Edited by* R.S. Sinha. Developments in Geotechnical Engineering, Elsevier Science Publishers, Amsterdam, 59A, pp. 203–262.

Einstein, H.H., Bischoff, N., and Hofmann, E. 1972. Behaviour of invert slabs in swelling shale. *In* Proceedings of the International Symposium on Underground Openings, Lucerne, Switzerland, pp. 296–319.

Franklin, J.A., and Hungr, O. 1977. Rock stresses in Canada: their relevance to engineering practice. Rock Mechanics, **6**: 25–46.

Grob, H. 1972. Schwelldruc im Belchentunnel. *In* Proceedings of the International Symposium on Underground Openings, Lucerne, Switzerland, pp. 99–119.

Hoek, E., and Brown, E.T. 1980. Underground excavations in rock. Institution of Mining and Metallurgy, London, U.K.

Huang, J.A. 1993. Long-term deformation behaviour of Queenston shale. M.E. Sc. thesis, University of Western Ontario, London, Ont.

ISMR Commission on Swelling Rock. 1994. Comments and recommendations on design and analysis procedures for structures in argillaceous swelling rock. International Journal of Rock Mechanics and Mining Sciences and Geomechanics Abstracts, **31**: 537–546.

Lee, Y.N. 1988. Stress–strain–time relationship of Queenston shale. Ph.D. thesis, University of Western Ontario, London, Ont.

Lee, C.F., and Lo, K.Y. 1976. Rock squeeze study of two deep excavations at Niagara falls. *In* Proceedings of the ASCE Specialty Conference on Rock Engineering Boulder, Colo., 15–18 August, pp. 116–140.

Lee, Y.N., and Lo, K.Y. 1993. The swelling mechanism of Queenston shale. *In* Canadian Tunnelling, Tunnelling Association of Canada, Toronto, Ont., pp. 75–97.

Lo, K.Y. 1978. Regional distribution of *in situ* horizontal stresses in rocks of southern Ontario. Canadian Geotechnical Journal, **15**: 371–381.

Lo, K.Y. 1986. Advances in design and performance evaluation. Keynote address in "Recent advances in Canadian tunnelling technology". *In* Proceedings of the 6th Canadian Tunnelling Conference, Niagara Falls, Ont., pp. 5–46.

Lo, K.Y., and Hefny, A. 1996. Design of tunnels in rock with long-term time-dependent and nonlinearly stress-dependent deformation. *In* Canadian Tunnelling, Tunnelling Association of Canada, Toronto, Ont., pp. 179–214.

Lo, K.Y., and Lee, Y.N. 1990. Time-dependent deformation behaviour of Queenston shale. Canadian Geotechnical Journal, **27**: 461–471.

Lo, K.Y., and Yuen, C.M.K. 1981. Design of tunnel lining in rock for long term time effects. Canadian Geotechnical Journal, **18**: 24–39.

Lo, K.Y., Wai, R.S.C., Palmer, J.H.L., and Quigley, R.M. 1978. Time-dependent deformation of shaly rocks in southern Ontario. Canadian Geotechnical Journal, **15**: 537–547.

Lo, K.Y., Lukajic, B., and Ogawa, T. 1984. Interpretation of stress-displacement measurements. *In* Proceedings of the Geotechnical Engineering Division/ASCE–GEOTECH'84, Atlanta, Ga., 14–16 May, pp. 128–155.

Lo, K.Y., Cooke, B.H., and Dunbar, D.D. 1986. Design of buried structures in squeezing rock in Toronto, Canada. *In* Proceedings of the 6th Canadian Tunnelling Conference, Niagara Falls, Ont.

Madsen, F.T., and Nüesch, R. 1991. The swelling behaviour of clay-sulfate rocks. *In* Proceedings of the 7th International Congress on Rock Mechanics, Aachen, Germany, pp. 285–288.

Trow, W.A., and Lo, K.Y. 1989. Horizontal displacements induced by rock excavation: Scotia Plaza, Toronto, Ontario. Canadian Geotechnical Journal, **26**: 114–121.

Wittke, W., and Pierau, B. 1979. Fundamentals for the design and construction of tunnels in swelling rock. *In* Proceedings of the 4th International Congress on Rock Mechanics, Montreux, A.A. Balkema, Rotterdam. Vol. 2, pp. 719–729.

Appendix A: an example for computing swelling strain

In this section the procedure used to calculate the swelling strain is described. To demonstrate this, the simulation results presented in Fig. 9 are considered, where an axial stress σ_y = 0.69 MPa is applied in the *y* direction. The parameters used in this simulation are listed in Table 1.

For an applied stress σ_y = 0.69 MPa in the *y* direction, the reduction ratios are calculated using eq. [3]

$$[A1] \quad R_{yy} = \frac{\log\left(\frac{\sigma_y}{\sigma_{th}}\right)}{\log\left(\frac{\sigma_c}{\sigma_{th}}\right)} = 0.767$$

No stresses were applied in the x and z directions of the sample (i.e., $\sigma_x = \sigma_z = \sigma_{th} = 0.001$ MPa).

$$[A2] \quad R_{xx} = \frac{\log\left(\frac{\sigma_x}{\sigma_{th}}\right)}{\log\left(\frac{\sigma_c}{\sigma_{th}}\right)} = 0.0$$

$$[A3] \quad R_{zz} = \frac{\log\left(\frac{\sigma_z}{\sigma_{th}}\right)}{\log\left(\frac{\sigma_c}{\sigma_{th}}\right)} = 0.0$$

The virtual stresses in the x direction corresponding to the reduction ratios are calculated using eq. [7] as

$$[A4] \quad \sigma^*_{xy} = \sigma_{th} 10^{[R_{yy}\mu_{xy}\log(\sigma_c/\sigma_{th})]} = 0.097 \text{ MPa}$$

$$[A5] \quad \sigma^*_{xz} = \sigma_{th} 10^{[R_{zz}\mu_{xz}\log(\sigma_c/\sigma_{th})]} = 0.001 \text{ MPa}$$

The values of $\mu_{xy} = 0.7$ and $\mu_{xz} = 0.65$ are used in eqs. [A4] and [A5] (see Table 1).

Therefore, the total stress in the x direction to suppress the swelling deformation is (eq. [8])

$$[A6] \quad \sigma_x^{TS} = \sigma_x + \sigma^*_{xy} + \sigma^*_{xz} = 0.099 \text{ MPa}$$

Now the reduction ratio R_x^{TS} is calculated using eq. [9].

$$[A7] \quad R_x^{TS} = \frac{\log\left(\frac{\sigma_x^{TS}}{\sigma_{th}}\right)}{\log\left(\frac{\sigma_c}{\sigma_{th}}\right)} = 0.54$$

Finally, the swelling potential, $m_{x(\sigma)} = 0.13$ has been obtained from eq. [10] under this stress condition in which the free swelling potential is $m_{x(0)} = 0.28$ (see Table 1). A similar technique has been used to calculate the deformation in different directions for other loading conditions (Figs. 9–12).

List of symbols

$m_{i(0)}$	free swelling potential in i direction
$m_{i(\sigma_{ij})}$	swelling potential in i direction under σ_{ij}
R_{ij}	reduction ratios
t	time
δ_{ij}	Kronecker delta
ε_i	swelling strain in i direction
$\varepsilon_{i(0)}$	free swelling strain in i direction
σ_c	critical stress after which there is no swelling strain
σ_i	principal stress in i direction
σ_{ij}	stress tensor
σ^*_{ij}	virtual stress in i direction for an external load in j direction
σ_{th}	threshold stress below which there is no stress effect on swelling
μ_{ij}	pseudo-Poisson's ratios